Research Article

Preparation of Nanosize Bone Powder from Waste and Development of Al Composite through Squeeze Casting Process

R. Muthu Kamatchi [ID],[1] R. Muraliraja [ID],[1] C. Sabari Bharathi [ID],[1] T. Sathish [ID],[1] S. Sathyaraj [ID],[1] and Leevesh Kumar [ID][2]

[1]*Department of Mechanical Engineering, Vels Institute of Science Technology and Advanced Studies, Chennai, India*
[2]*Department of Construction Technology and Management, Ambo University, Ambo, Oromia, Ethiopia*

Correspondence should be addressed to Leevesh Kumar; leevesh.kumar@ambou.edu.et

Al6061 alloy is most commonly used in automotive, marine, and aerospace applications to lighten the composite and increase its strength. Al6061 alloy is a precipitation-hardened aluminum alloy used as a matrix material. Beef bone is a biowaste that has polluted the environment and the people who live in the vicinity of its manufacturing and disposal sites. Biowaste has been used in a variety of ways by researchers in recent years, including activated carbon, water purification, reinforcement in composites, fillers, additives, etc. Beef bones that had been abandoned as waste were collected, cleaned, and grounded into a fine powder with a particle size of 50–100 nm and used as reinforcement. Squeeze casting process is used to create the newly created aluminum composite (Al6061 + 0%, 5%, 10% of bone powder). The aluminum composite was fabricated and three samples were successfully obtained for further testing and analysis. The prepared Al composites with nanopowder reinforcement are analyzed for surface morphology, elemental identification, hardness, porosity, tensile strength, and compression strength. The percentage of porosity in the composite is improved by 36.7% when compared to the Al6061 alloy. Similarly, the tensile strength of the produced composite is increased to 5.59%. A significant improvement is observed in the wear resistance and hardness of the composite as 54.55% and 48.65%, respectively.

1. Introduction

Aluminum matrix composites (AMCs) are high-tech materials with remarkable characteristics. AMCs are made up of numerous materials, one of which is aluminum, which may be improved by combining them [1]. Aluminum alloys are being phased out of many uses in the automotive, aerospace, marine, and nuclear sectors [2]. Heavy-duty industrial applications need lightweight materials with high specific stiffness, strength, and heat resistance, and metal matrix composites (MMCs) like the Al600 series (Al6061/6063) fit the bill. The casting method for MMCs can be used to produce near-net form composites at a low cost [3]. Particle-reinforced Al MMCs are well-suited for use in the aerospace, automotive, military, and leisure sectors because of their unique mixture of features [4]. Their characterization has been hampered by unknown properties such as wettability, adsorption properties, chemical compatibility, and the development of complex

stress states as a result of changes in temperature and moisture expansion [5]. AMCs have partially achieved this goal because of their excellent qualities such as stiffness, low density and high damping, enhanced wear resistance, and simplicity of production [6]. It is possible to enhance the performance of Al–Si alloys by altering the particle size, shape, and content of Si particles. Al–Si cast alloys may also be strengthened with hard ceramic reinforcements such as Al_2O_3, SiO_2, ZrB_2, SiC, TiC, and B_4C to boost their performance even more. Adding hard-ceramic particles to composites improves their performance but their greater cost raises the whole cost. Red mud, bagasse ash, fly ash, rice husk ash (RHA), eggshells (ESs), and other industrial wastes are used as efficient aluminum alloy-reinforcing materials. Many researchers have reported better physical, mechanical, and thermal characteristics with the effective use of these materials as reinforcement [7]. Air and soil pollution are major concerns all around the globe. Typically, industrial waste is the

TABLE 1: Mechanical properties of composite material prepared using various organic reinforcements.

Sl. no.	Matrix	Reinforcement	Hardness	Compression or tensile	References
1	Al6061	Rice husk	48.4 BHN	171.3 MPa (T)	[10]
2	AMC	Aloe vera	33.8 BHN	119.83 MPa (T)	[11]
3	Al6082	Red mud	95 HV	169.87 MPa (T)	[12]
4	Al7075	Coconut shell fly ash	169.5 BHN	189 MPa (T)	[13]
5	Al6063	Fly ash	86 BHN	169 MPa (T)	[14]
6	Al2024	Eggshell	109 BHN	208.9 MPa (T)	[15]
7	Al6061	Eggshell	103 HRC	138.62 MPa (T) 351.22 MPa (C)	[16]
8	Al7075	Rice husk	121 HV	260 MPa (T) 563 MPa (C)	[17]
9	Al356	Fly ash	88.45 BHN	320.65 MPa (T)	[18]
10	Al2025	Red mud	79.99 HV	186.42 MPa (T)	[19]

source of this form of pollution. Agricultural and industrial wastes such as cement, red mud, fly ash, ESs, rice husks, coconut shells, and bagasse may be used to reduce the processing costs of composites [8]. The presence of $CaCO_3$ in ESs demonstrates its ability to enhance the mechanical characteristics of any material when used as reinforcement. ES may serve as a useful reinforcing material when working with aluminum to improve the properties [9]. The mechanical properties of composite materials are collected from the previous research work, as shown in Table 1. The organic waste materials were prepared, and composites were prepared for various applications. Many researchers reported that the addition of prepared particles elevates the properties of the composite when compared to the Al alloy.

Dwivedi and Srivastava [7] postulated that collagen powder and Al_2O_3 ceramic particles serve as major reinforcement with aluminum as a basic material. The results of the microstructural investigation indicate homogeneous distribution of collagen powder and Al_2O_3 particles in the matrix material. Tensile strength was increased by 14.32% by incorporating 5% Al_2O_3 and 1.25 wt% collagen powders into the aluminum matrix material. The addition of 6.25 wt% Al_2O_3 to aluminum resulted in a 35.29% increase in hardness. It was also discovered that adding 2.5 wt% Al_2O_3 and 3.75 wt% collagen powder to aluminum at the same time increased its durability by 27.77%. For further confirmation of the existence of Al_2O_3 and Cr, an X-ray diffraction investigation was also carried out. Aluminum alloy 6,063 was strengthened with different weight percentages from 2.5% to 12.5% of palm kernel shell particles. In a permanent mild steel mold, a stir casting process was used to create the composite. The morphological study revealed that the secondary phase of palm kernel shell reinforcements was disseminated uniformly in the main phase of the aluminum matrix. The incorporation of palm kernel shell particles into the composites resulted in a higher density and greater porosity than the basic alloy. The development of composites revealed the formation of intermetallic compounds [20]. Imran and Anwar Khan [21] investigation have been carried out on alloys and reinforcements that are used to fabricate aluminum metal matrix composite (AMMC) materials. According to the findings, a mechanical property

has improved significantly. Low coefficient of thermal expansion was compared to standard base alloys; superior wear and corrosion resistance. In their research, Omoniyi et al. [22] looked at physical and mechanical factors such as density, impact strength, tensile strength, hardness, and microstructure. The density reduces as the proportion of reinforcement increases. 97.69 MPa is the highest ultimate tensile strength (UTS) of the aluminum–wood composite, whereas 40.189 MPa is the maximum UTS of the unreinforced aluminum alloy. There are wide variations in impact energy, with a maximum of 89.00 J at 10% weight of wood particle addition but the hardness is more or less constant, ranging from 52.33 to 62.0 BHN at 10% weight. The aluminum–wood composite had better mechanical qualities than pure aluminum in all of the mechanical tests. According to the microstructure study, the wood particles were evenly dispersed in the MMC. Saravanan and Senthil Kumar's [23] work showed the possibility of strengthening aluminum alloy (AlSi10Mg) using locally accessible and affordable RHA for the development of a novel material. Liquid metallurgy was employed to generate MMCs with a RHA particle content of 3%, 6%, 9%, and 12% by weight. According to the findings, increasing the proportion of RHA reinforcement increases the composite's ultimate tensile, compressive, and hardness strength. Islam et al. [24] explained the synthesis of industrial and agricultural wastes loaded onto AMMC, as well as their mechanical, corrosion, and physical properties. Innovative filler particles that are inexpensive, accessible, and have better properties than standard particles are discussed in this study. An electron microscopic image of the hybrid composite, as well as measurements of density and hardness, was used to verify its validity. The surface hardness of the composite with 6% ES powder produces a hardness value of 197 HV. Calcium oxide, which is tougher than carbide particles reinforced in the hybrid composite material, is the type of biological ES found in it. The hybrid composite with 3% SiC and 6% ES has high wear resistance, so it is a suitable choice for construction. A hybrid composite containing 6% of Al_2O_3 and 6% of SiC has good adhesive morphology and shows less wear. So, it has been found that a decrease in hard particles or an increase in ES could affect sliding wear [25]. According to Ikubanni et al. [26], hybrid-reinforced AMCs were explored
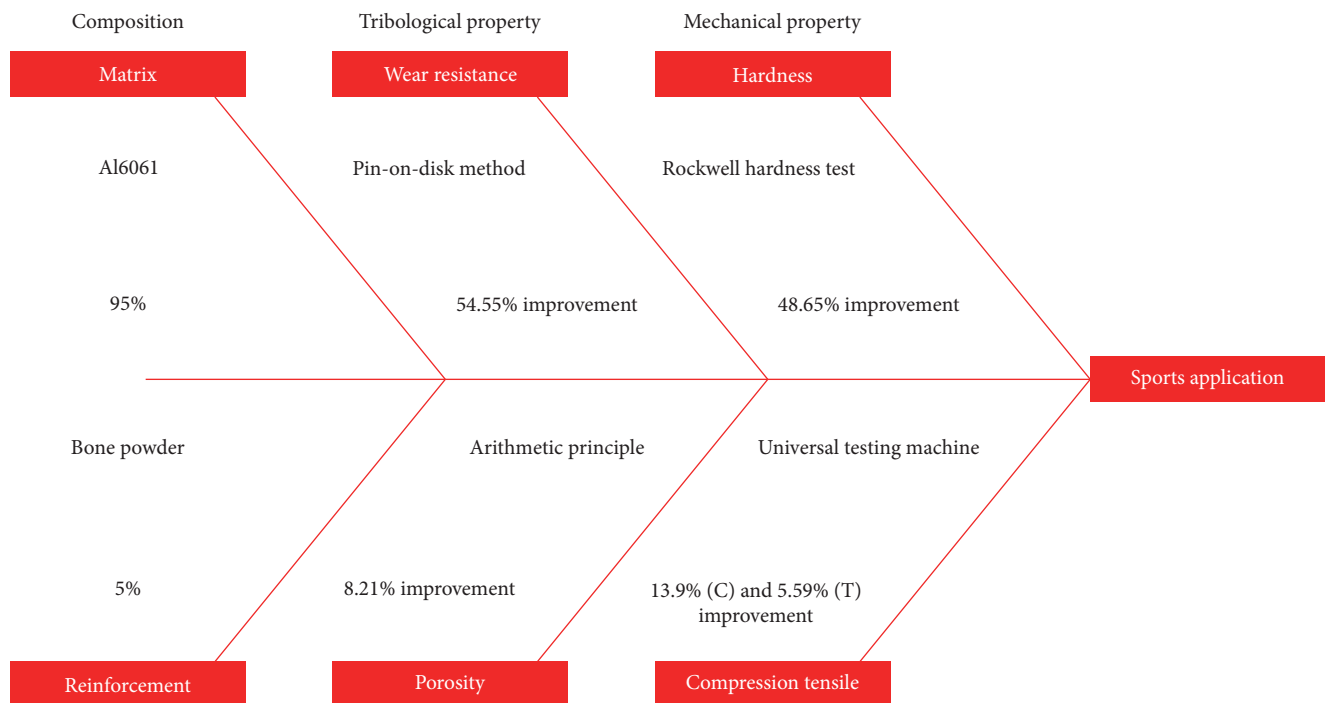
FIGURE 1: Fishbone diagram for research work carried out.

by using Al6063 alloy, SiC, and palm kernel shell ash (PKSA) reinforcements. With the use of the double stir casting process, different amounts of SiC and PKSA were incorporated into the matrix metal at various ratios. During the experiments, the samples' densities and porosities were assessed. The findings showed that the density of the composite decreased with an increase in PKSA, whereas the density improved in other samples with an increase in SiC. Double stir casting process yielded appropriate porosity percentages for cast MMCs, as shown by the findings, which revealed that the percentages of fell were within the allowable range. Verma and Kumar [27] have found that using rice husk and fly ash to generate an AMMC results in increased quality, including physical and superior wear resistance abilities. The primary objective is to evaluate the feasibility of using the stir casting method to make aluminum alloys with the specified reinforcements. The machinability of the material has been examined via the use of electrical discharge machining (EDM) tests, and analysis of the agrowaste and fly ash distribution in aluminum composites has been done by scanning electron microscopy (SEM). Composites have also been studied for their mechanical and corrosion characteristics. According to Yadav et al. [28], adding RHA to an aluminum alloy matrix improves the mechanical and physical characteristics and increases the wear rate resistance of the composite. Composites' scanning electron micrographs reveal a uniform distribution of grain ash in the aluminum matrix. When exposed to high temperatures, aluminum alloys lose their microcutting properties and begin to oxidation. The composite material's strain fields and wear resistance are enhanced because of the difference in coefficients of thermal expansion between the matrix and reinforcing materials. Yadav et al. [29] created AMMCs using ES and RHA reinforcements. In the AMMC study, ES and RHA reinforcements at

4.75 and 1 wt% Cr increased tensile strength and hardness by 22.41% and 45.5%, respectively. There are no data available regarding the bone powder used as reinforcement. However, it is also found that most of the waste materials used as reinforcement, so far, improve the strength of the material.

Thus, in this research work, new material composition is formulated and developed using the squeeze casting process. Al6061 alloy is used as as matrix material, which is the most commonly used material in sports applications. For the first time, the bone powder is prepared and used as reinforcement to produce the new Al composite. The morphological study is done using a scanning electron microscope and the presence of added elements is identified through energy dispersive X-ray (EDAX) analysis. The percentage of porosity is measured using the arithmetic principle for the composite. A hardness tester, a universal testing machine, and a pin-on-disk tribometer are used to check the finished composite. The overview of the work is given with the help of a fishbone diagram for better understanding, as shown in Figure 1. The composition of the matrix in this work is Al6061 at 95%, and the reinforcement material is beef bone powder at 5%, produced using the squeeze casting process. The physical properties of the composites, such as porosity and hardness, are improved by 36.7% and 48.6%, respectively. The mechanical properties such as tensile and compression strengths of the composites are improved by 5.59% and 13.97%, respectively. The tribological properties of the composites were improved by 54%, and measured using the pin-on-disk method.

2. Experimental Details and Procedures

2.1. Matrix and Reinforcement Materials. The matrix material, aluminum Al6061, was procured from the metal market.

TABLE 2: Chemical composition of Al6061.

Element	Mn	Fe	Mg	Si	Cu	Zn	Ti	Cr	Other	Al
%	0.15	0.70	1.20	0.80	0.40	0.25	0.15	0.35	0.05	Balance

TABLE 3: Chemical composition of beef bone.

Element	CaO	P_2O_5	MgO	SiO_2	Others
%	48.21	37.77	1.29	0.12	12.61

TABLE 4: Squeeze casting process parameters used for the fabrication of composites.

Sl. no.	Process parameters	Recommended conditions	References
1	Squeeze pressure	100 MPa	[30]
2	Squeeze pressure holding time	45 s	[31]
3	Melting temperature	700°C	[32]
4	Die temperature	250°C	[33]
5	Stirring time	5 min	[34]
6	Stirring speed	600 rpm	[33]
7	Reinforcement percentage	5% (in μ)	[35]
8	Reinforcement preheating temperature	300°C	[35]

Composites were developed using waste cow bone, which was gathered from a butcher market and used as reinforcing material. The bones were initially cleaned with sufficient amount of water to remove the skin and then cleaned with acetone. The collected bones were bigger in size, to make it into smaller size, portable hand wheel cutter made it as powder using grinder machine. Finally, it was reduced to nanosize using ball milling machine. A portable X-ray fluorescence (XRF) analyzer was used to determine the Al6061's elemental makeup, as shown in Table 2. Table 3 shows the composition of reinforced waste beef bones.

2.2. Production of MMCs using the Squeeze Casting Method. Using the squeeze casting procedure, the composites were made, and the parameters employed in this study are shown in Table 4. To eliminate filth and oil, an aluminum rod was procured from the market and cleaned with acetone. To make it fit through the crucible's entry, the rod was sliced into small pieces. In the beginning, 300°C was applied to the permanent hardened steel dies measuring 50 mm in diameter and 250 mm in length. To keep the melt temperature at 700°C, the pressure-casting furnace with temperature control was turned on and set to 750°C. A nonstick boron carbide coating was then applied to the stirrer rod and stirrer, which was then cured at 250–300°C to protect the stirrer edges from deterioration at high temperatures. At 300°C, the preheating chamber warmed the reinforcement particles so that they would be free of moisture and clump together less easily. When the crucible temperature reached 350°C, the matrix materials were loaded into the furnace and subsequently heated to 700°C, at which point the alloy fully melted. It was then time to turn on the stirring rod and place it 30 mm above the bottom of the reaction vessel with its stirring speed set to 600 revolutions per minute. Magnesium (1 wt%) was added to

the molten matrix to increase the wettability between the matrix and the reinforcement. A 5-min stirring period followed the addition of the warmed reinforcement particles. A bottom tapping mechanism was used to transport the molten mixture into the preheated route pipe that was linked to the die of the squeeze casting system. The molten liquid was squeezed at 100 MPa for 45 s after it was put onto the prepared die at 250°C. The following three samples were made using the same method. Squeeze casting process parameters for the AMCs are shown in Table 4.

2.3. Microstructural and Elemental Composition Characterization. Using an automated mounting press, samples were trimmed to the desired size and then mounted (Buehler SimpliMet 1000). A Buehler AutoMet 250 was used to grind and polish the samples. Using 400, 600, and 1,200 grit abrasive papers, three phases of diamond suspension were used to physically polish the surface for 5 min. The samples were etched using Keller's reagent using the ASTM E3-01 standard. The KEYENCE optical microscope 1,000x VHZ100R was used for surface morphological examination. A field-emission scanning electron microscope (FESEM) (JEOL JSM-7600F) with an associated energy-dispersive spectroscopy was used to investigate the samples' microstructures, elemental composition, and fracture and wear analyses. The Panalytical Axios Max machine was used to perform XRF investigations of the matrix and reinforcement to determine their composition.

2.4. Porosity Measurement. Porosity of AMC was quantified by measuring the density of the matrix and reinforcement. Measurements were made using the Archimedes method using a sample size of 30 mm in length by 10 mm in breadth and 3 mm in thickness. A rule of the mixture was used to compute the theoretical density of composites [18]. According to Equation (1), the samples' porosity is calculated.
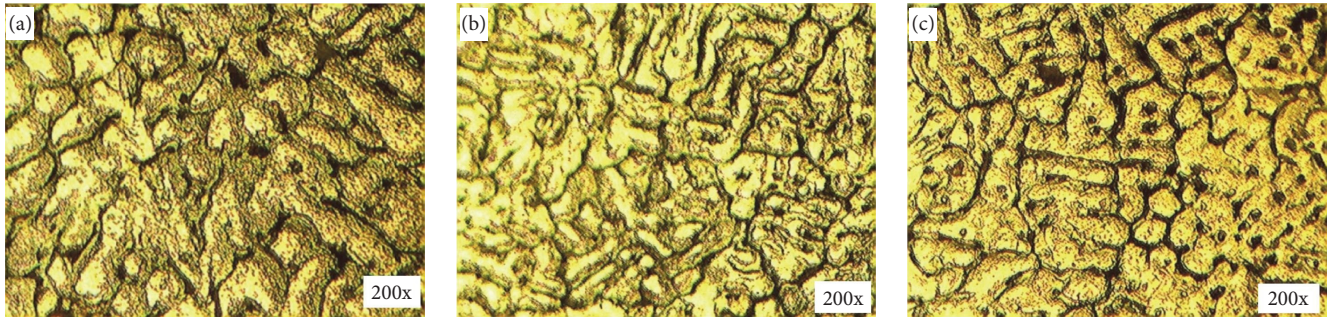
FIGURE 2: Optical micrograph captured at 200x magnification of AA6061 prepared with various percentages of reinforcement: (a) 0% bone powder; (b) 5% bone powder; (c) 10% bone powder.

$$P = 1 - \frac{\rho_{\text{experimental}}}{\rho_{\text{theoretical}}} \times 100. \tag{1}$$

2.5. Mechanical and Wear Characterization. The samples were subjected to tests to determine their hardness, compressive strength, tensile strength, and wear resistance. Using a Universal Hardness Tester (UH250), the indentation method was used to determine the hardness of the material under test. The standard deviation value was calculated based on five repeated observations taken at different sites. At room temperature, according to the ASTM B647 standard, the hardness is measured using Vicker's hardness testing apparatus. The 0.5 kgf weight is applied using the indenter for 15 s. The average of three readings from five indentations is chosen as the hardness value. The tensile load was applied to the specimen while it was held in place by the specimen's two ends. Using the machine's stress–strain curve, mechanical characteristics like yield and ultimate stress were determined for the samples. The tensile test's strain rate was 8.33 10-4/s. A 100 kN universal testing machine was used to perform compression tests in accordance with ASTM E9. Cylindrical samples with a diameter and height of 20 mm and a crosshead speed of 1 mm/min (a strain rate of about 8.33 10-4/s) were used for the uniaxial compression testing. Each sample was allowed to compress to 10 mm or half its height before the load-stroke data were transformed into the stress–strain curves and the results were compared. A pin-on-disk tribometer is used to assess the manufactured composites' particular wear rate while applying a 10 N load. The sample's 10 mm diameter and 30 mm height were prepared for this analysis. Stainless steel with a high carbon and high chromium content is employed as the analysis' counterpart. The sample's initial and final weights are taken into account to calculate the sample's weight loss. The formula is used to compute a certain wear rate (w).

$$w = \Delta V / (L \times d), \tag{2}$$

where ΔV is the volume loss (in mm^3), L is load (in Newton), and d is the sliding distance (in m).

3. Results and Discussion

3.1. Characterization of Microstructure and Elemental Composition in Composites. Images of three distinct composites at 200x magnification are shown in Figure 2(a)–2(c). In the images, dark parts are reinforcements, white portions are Al matrix, and black regions are porosity flaws. At grain boundaries, all-optical microstructures have a morphology that is practically nondendrites due to the squeezing pressure, resulting in finer dendrite and smaller dendrite arm spacing [36]. From the microstructure, as shown in Figure 2(b), it can be seen that the composites have reinforcement with approximately uniform dispersion and a dense structure without microlevel voids, thanks to the inclusion of pure bone. Figure 2(c) shows that although certain bone particles were clustered together, the overall distribution of the particles was homogeneous, as shown in Figure 2(b). It demonstrates that increasing the amount of bone in the aluminum matrix results in increased porosity on the samples. This is due to the longer particle feeding time, which increases the amount of time the particles are in contact with the air [37].

Figure 3 shows the 1,000x magnifications of the FESEM images of the three samples. The distribution of reinforcement in the matrix of the composite material is visible on the microscope. The matrix and reinforcement are represented by the bright and dark particles, respectively. Figure 3(b) shows that the 5% reinforcement particles were effectively disseminated in the matrix but some tiny clusters were remained in the microstructure, and also shows a uniform particle distribution in a 5% reinforcement composite. Reinforcement particles with a 5% content were distributed along the grain boundaries of the aluminum matrix. An intergranular distribution on grain boundaries improves mechanical characteristics and avoids grain boundary failure. Figure 3(c) shows the 10% reinforcement composites with distributing the reinforcements equally across the sample. However, it is produced with a higher percentage of porosities. The elements in the composite are identified using EDAX analysis, as shown in Figure 4. From the analysis, the percentage of added elements as reinforcement is found in the sample, as shown in Figures 4(b) and 4(c), with the variation in the percentages. As shown in Figure 4(a), the Ca percentage is 0% as the sample 1 is not added with reinforcement.
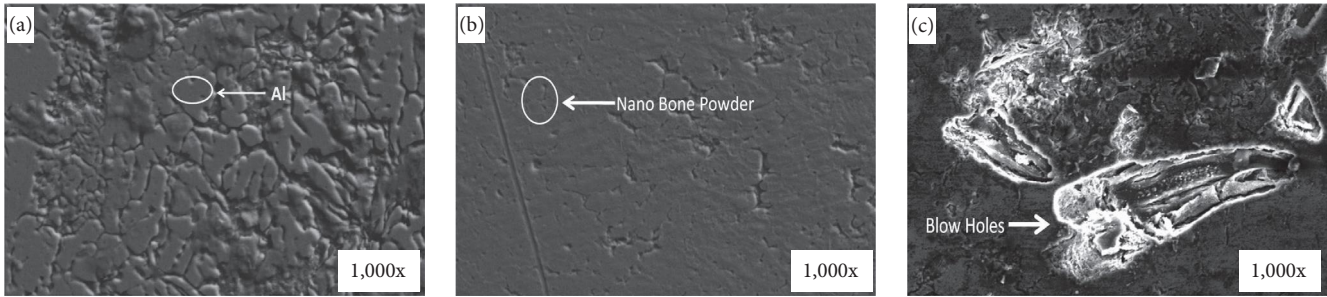
FIGURE 3: Field-emission scanning electron microscope images of the three composites: (a) without reinforcement; (b) 5% reinforcement; (c) 10% reinforcement.

3.2. Physical Properties of the Composite.

The distribution of reinforcements, pore size, and other factors all have a role in how porous a material is. When the porosity is low, there are fewer empty areas in the composite material, which increases its strength. The computed porosity findings are in agreement with the optical microscopy results. As shown in Figure 5, the 5% composite sample shows very little porosity, while samples that have 10% reinforcement exhibit high porosity. In squeeze casting process, increased solidification pressures help in excellent die filling, decreasing casting flaws, notably porosity. Figure 5 shows that with the experimental density, the squeeze casting technique is quite effective in producing experimental densities that are very near to theoretical densities [38]. As shown in Figure 5, it is also evident that the strength of the 5% reinforcement could be highest, followed by 10% due to the increase in the porosity in the sample which has 10% reinforcement.

Table 5 shows the hardness values of all the produced composites. From the obtained results, it can be concluded that the composite (Al6061 + 5% bone powder) is the hardest one, followed by the Al6061 + 10% bone powder composite, as shown in Figure 6. The Al6061 + 0% bone powder is found to be the least hard material, followed by the Al6061 + 10% bone powder composite. The maximum hardness of 105.1 HV is achieved for the Al6061 + 5% bone powder composite because of the lower porosity and uniform distribution of reinforcements in the matrix, especially at the grain boundaries. The porosity test also confirmed less porosity in the Al6061 + 5% bone powder sample. The grain size in the composite is also relatively smaller, as it is evident in the optical microscope images. With the decrease in the grain size, the hardness of the material increases [39].
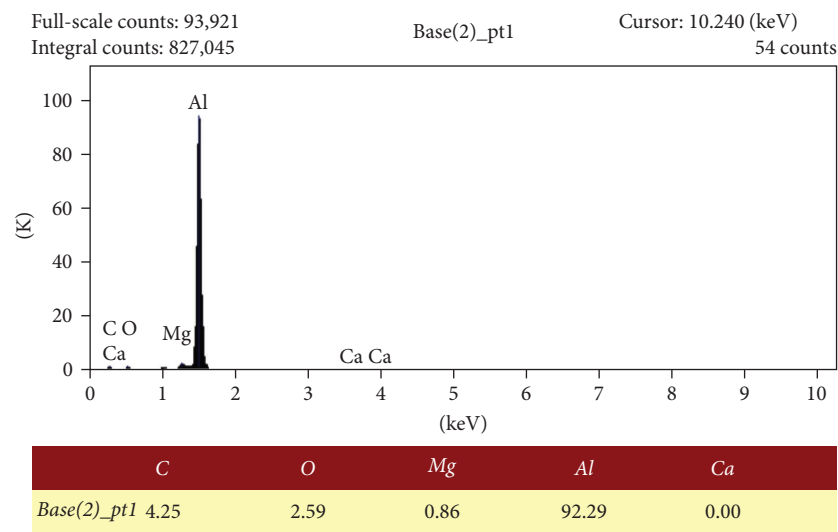
3.3. Characterization of Mechanical and Tribological Properties.

As shown in Figure 7, three distinct kinds of composite materials exhibit varied strain/tension relationships. These stress–strain curves reveal the tensile qualities such as elongation to fracture (ε_f), yield strength (σ_y) and UTS (σ_{uts}). The σ_y of Al6061 without bone has been found to be 106.26 MPa. The σ_{uts} of Al6061 without bone is 127.53 MPa with ε_f of 3.88%. The tensile characteristics of Al6061 without bone were found to be superior to those of other combinations. In the case of Al6061 + 5% bone, the values for σ_y, σ_{uts}, and f are 112.4, 134.6 MPa, and 2.48%, respectively. Al6061 + 5% bone recorded the predominant tensile characteristics in

comparison to other sample combinations. The data observed using the stress–strain curve are plotted and given in Figure 8. The sample which has Al6061 + 5% reinforcement shows high tensile strength and less porosity, as clearly seen in the micrograph and the computed percentage of porosity. The most ductile specimen was Al6061 + 5% bone, which was followed closely by Al6061 + 10% bone. As a result, bone reinforcement is more evenly distributed in the matrix, which may have contributed to the reduced porosity.
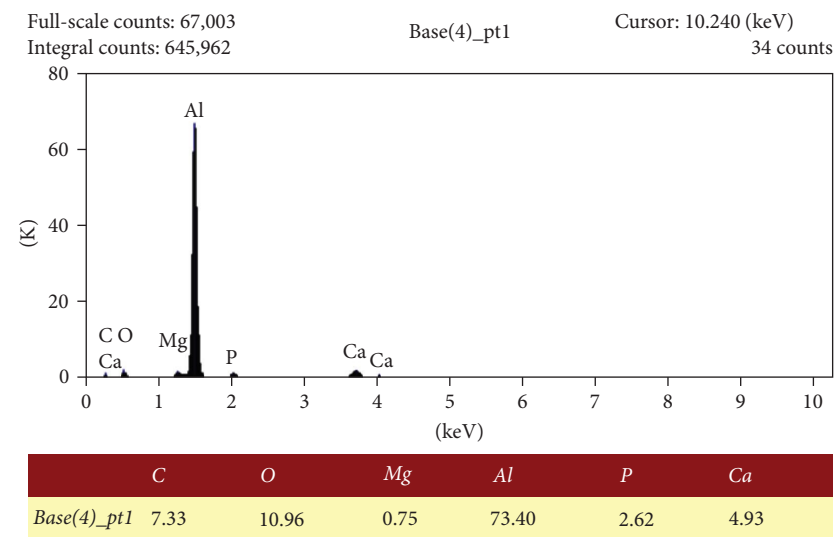
A compression test was conducted to establish the samples' compressive and fracture characteristics. A barrel-like deformation or bulging was detected in all samples, and this persisted until the samples formed a pancake shape. Figure 9 shows the load versus displacement curves derived from compression experiments. It is observed that Al6061 + 5% bone exhibited the highest ultimate stress of 212.2 MPa at a deformation of up to 6.9 mm from the original length. The break load of 28.3 KN has been measured and shown in Figure 10. It is notable that after the fracture initiation, the curve tends to proceed upward. The ultimate stress for Al6061 + 10% bone is roughly 165 MPa at a deformation of 6.7 mm and a break load of 21.94 KN. Al6061 + 10% bone has a poorer load-bearing capability than Al6061. In the compressive response of a 10% composite, a greater hardening rate in the Al6061 alloy matrix is observed. According to the results, 186 MPa was measured to be the ultimate stress in Al6061 without reinforcement composite at a deformation of 7.1 mm from the original length. This corresponds to the porosity seen in micrographs and the percentage of porosity.

As a function of sliding distance, the weight loss in the samples is calculated, and the weight loss is then used to compute the specific wear rate of the manufactured composites, which is shown in Figure 11. The composites containing Al6061 + 5% bone powder exhibit a low rate of wear. The waste bone particles in the composite protect the composite's surface by creating a scratching action on the material's counter surface. The resistance is proportional to the amount of hard waste bone on the surface of the composite sample. Figure 12 illustrates the wear trends of the produced composites.
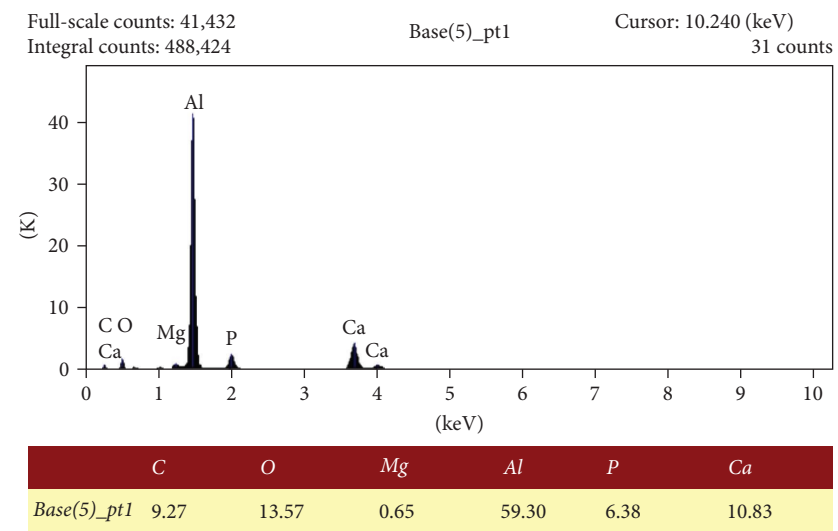
The frictional force of composite material is shown in Figure 13. Tribofilm generation at the pin/disk contact gives the samples a higher coefficient of friction (COF) value. Increase in applied load lead to an increase in the contact area, which in turn leads to a rise in the force needed to break them and, hence, an increase in COF. Other studies have

Full-scale counts: 93,921
Integral counts: 827,045

Base(2)_pt1

Cursor: 10.240 (keV)
54 counts

	C	O	Mg	Al	Ca
Base(2)_pt1	4.25	2.59	0.86	92.29	0.00

(a)

Full-scale counts: 67,003
Integral counts: 645,962

Base(4)_pt1

Cursor: 10.240 (keV)
34 counts

	C	O	Mg	Al	P	Ca
Base(4)_pt1	7.33	10.96	0.75	73.40	2.62	4.93

(b)

Full-scale counts: 41,432
Integral counts: 488,424

Base(5)_pt1

Cursor: 10.240 (keV)
31 counts

	C	O	Mg	Al	P	Ca
Base(5)_pt1	9.27	13.57	0.65	59.30	6.38	10.83

(c)

FIGURE 4: EDAX images of the three composites: (a) without reinforcement; (b) 5% reinforcement; (c) 10% reinforcement.
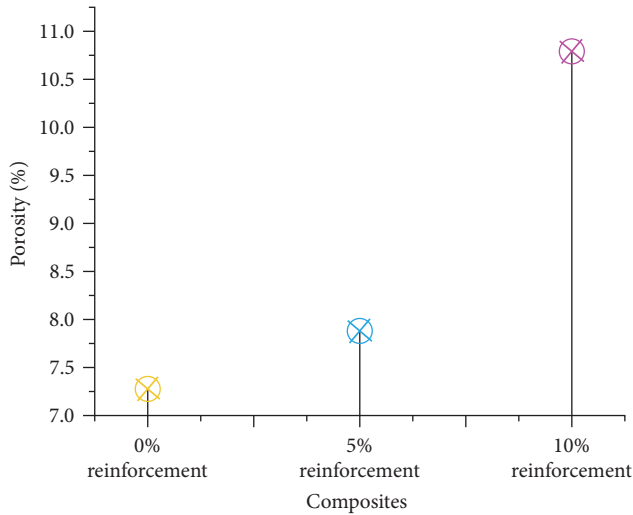
FIGURE 5: Percentage of porosity in the composites.

TABLE 5: Hardness values of produced composites.

Sample Id (%)	Hardness values in HV @ 0.5 kgf		
0	67.5	68.9	70.7
5	103.2	104.8	105.1
10	97.6	85.5	84.7
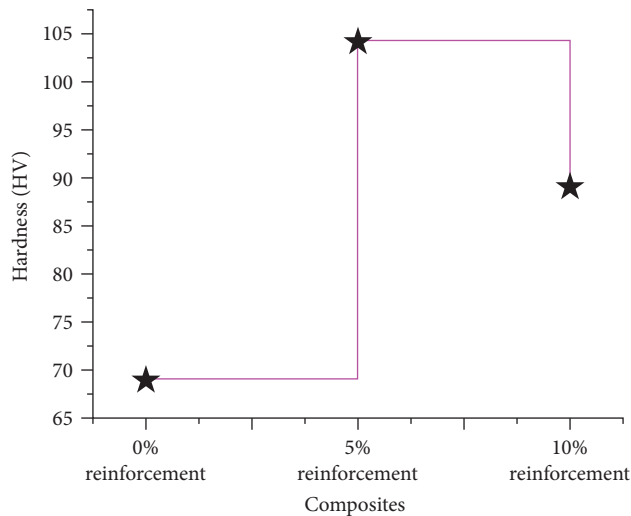
FIGURE 6: Hardness values of produced composites.

FIGURE 7: Tensile stress–strain curves of the composites.
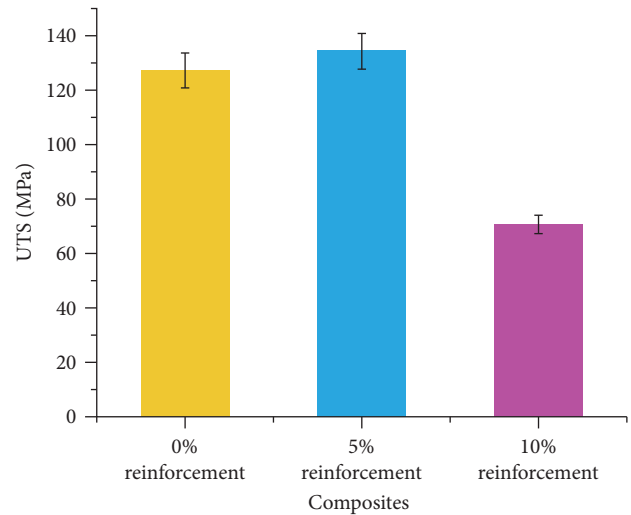
FIGURE 8: Ultimate stress of the various samples prepared.

made similar findings [40]. Archard's equation captures the relationship between wear rate and hardness, according to which a material's hardness has an inverse correlation with its wear rate. Since the wear surface contains greater resistance and bone particles that are hard, the material has a higher rate of wear [41].

According to the findings, bone particles are far more efficient than alumina in resisting penetration and cutting into the sur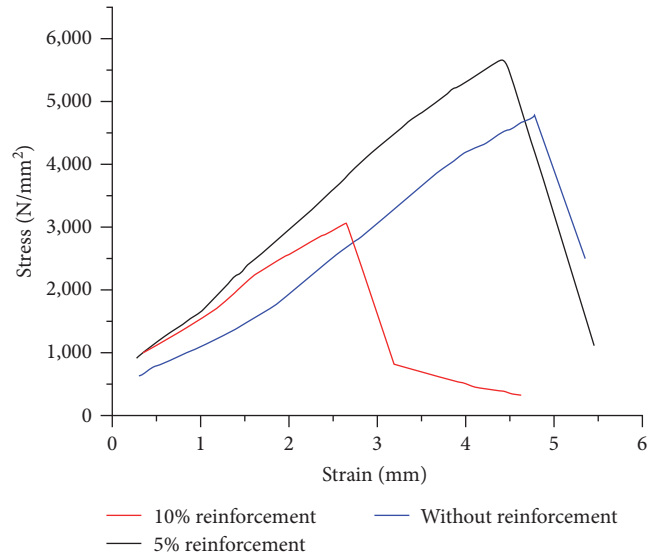face. It has been shown that an abrasion wear mechanism exists in the composite surfaces [12, 13]. It is observed that the reinforcement of 5% bone improves the abrasion and wear resistance of the aluminum composite. The reinforcing particle slows the rate of wear by shrinking the abrasion between the contact surfaces [42]. As a result, asperities are generated from the harder and softer surfaces of the materials. This mechanism of three-body abrasion wear mechanisms increases the surface roughness and frictional force values. The SEM topography of the wear track is shown in Figure 14. The topography of the region was seen to have narrow grooves, material flow, a greater degree of wear, and localized adhesion, as well as other characteristics that were observed. There are some ploughing and cutting effects in the wear pattern of all composites [43]. Plastic deformation is the predominant mode of wear in all composites. The ploughing effect is predominant in the topography of the composites, which have 10% reinforcement.
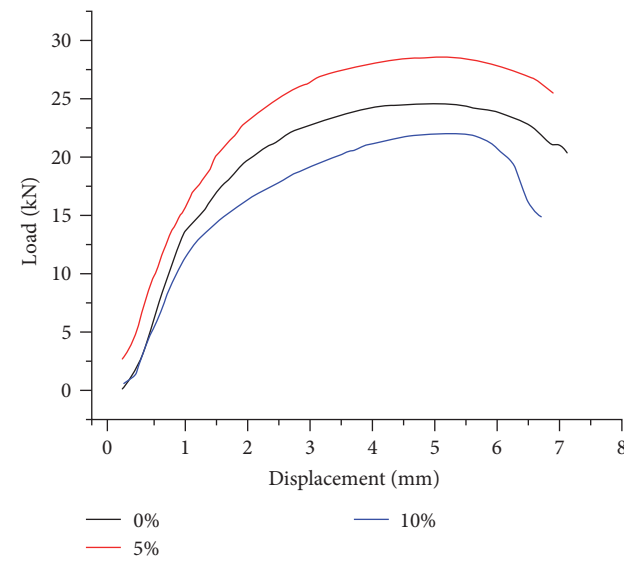
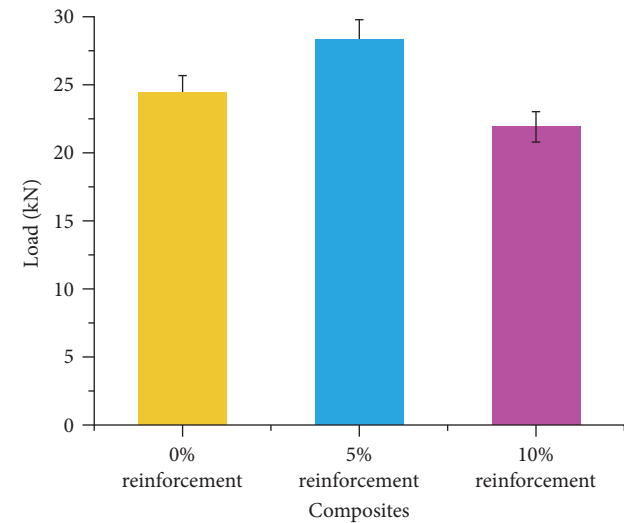FIGURE 9: Load and displacement curve of the composites.

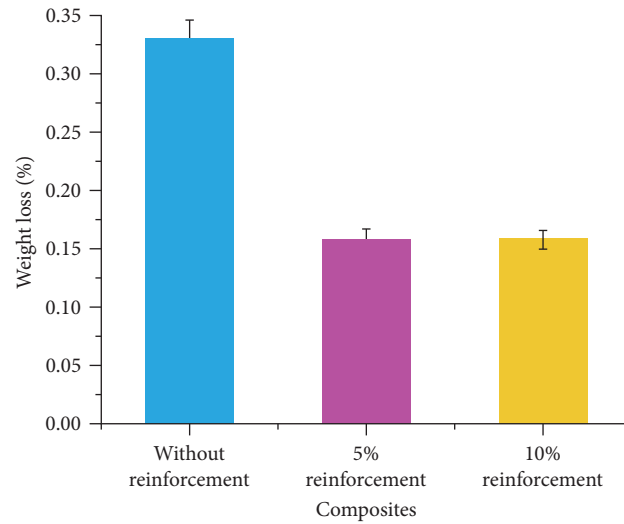FIGURE 10: Maximum load obtained on the composites.
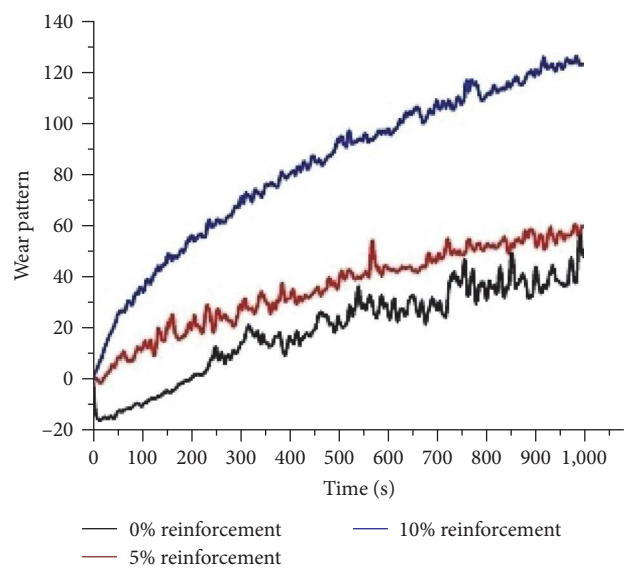

FIGURE 11: Weight loss in composites.

FIGURE 12: Wear pattern of the composites.
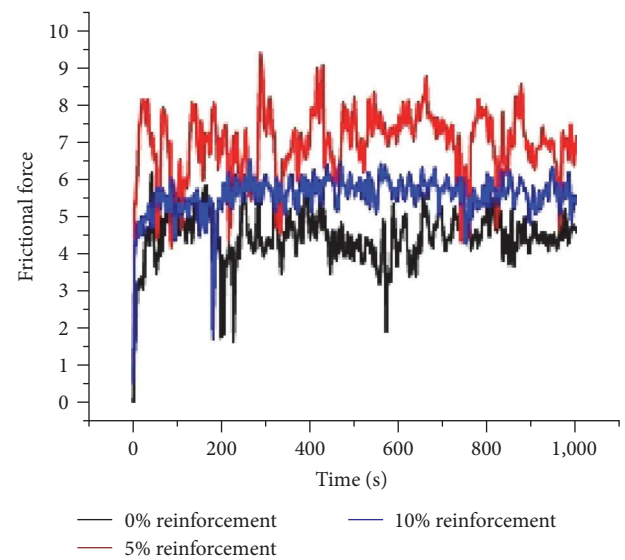
FIGURE 13: Frictional force versus time.

4. Conclusion

The outcomes of the data collection have led to the following conclusions:

(1) The SEM examination has shown the production of a novel star structure for the first time using bone powder, and the existence of elements added has been confirmed by elemental analysis.

(2) The composite's porosity has grown from 7.9% to 10.8%, which is a good improvement. The porosity in the composites was disclosed by optical microscopy.

(3) In comparison to the 6061 aluminum alloy, the hardness value of the composite increased by a substantial amount from 70.7 to 105.1.

FIGURE 14: Wear track of the composites: (a) without reinforcement; (b) 5% reinforcement; (c) 10% reinforcement.

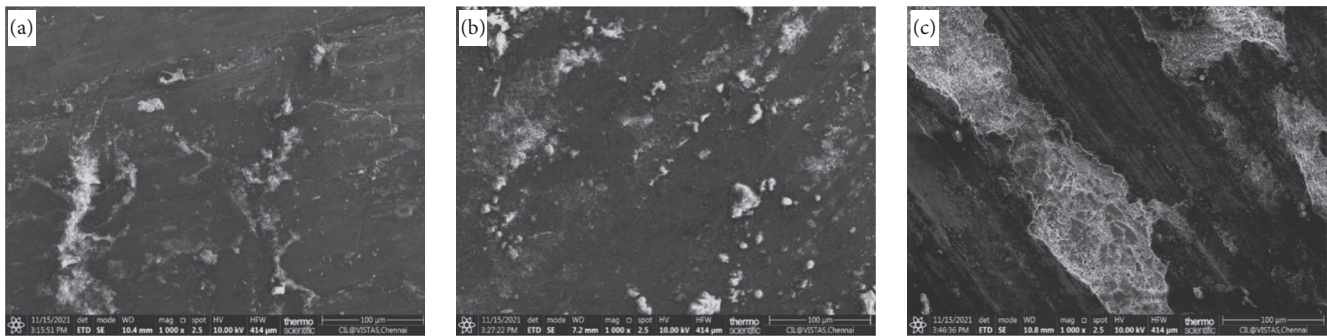(4) When compared to aluminum alloy, the composite's tensile strength is greatly enhanced, reaching 127.53–134.67 MPa, and the compression strength of the composite is marginally improved, reaching 186–212 MPa.

(5) The increased hardness value of the beef bone powder reinforcement composite may be reason for improvement in wear resistance up to 54.55%.

According to the findings of this study, the development of composites has substantially improved the physical, mechanical, and tribological characteristics of aluminum composites.

Data Availability

The data used to support the findings of this study are available from the corresponding author upon request.

Conflicts of Interest

The authors declare that they have no conflicts of interest.

References

[1] H. I. Akbar, E. Surojo, and D. Ariawan, "Investigation of industrial and agro wastes for aluminum matrix composite reinforcement," *Procedia Structural Integrity*, vol. 27, pp. 30–37, 2020.

[2] I. Dinaharan, R. Nelson, S. J. Vijay, and E. T. Akinlabi, "Microstructure and wear characterization of aluminum matrix composites reinforced with industrial waste fly ash particulates synthesized by friction stir processing," *Materials Characterization*, vol. 118, pp. 149–158, 2016.

[3] P. P. Kulkarni, B. Siddeswarappa, and K. S. H. Kumar, "A survey on effect of agro waste ash as reinforcement on aluminium base metal matrix composites," *Open Journal of Composite Materials*, vol. 9, no. 3, pp. 312–326, 2019.

[4] S. Rama Rao and G. Padmanabhan, "Fabrication and mechanical properties of aluminium–boron carbide composites," *International Journal of Materials and Biomaterials Applications*, vol. 2, no. 3, pp. 15–18, 2012.

[5] Z. Haktan Karadeniz and D. Kumlutas, "A numerical study on the coefficients of thermal expansion of fiber reinforced composite materials," *Composite Structures*, vol. 78, no. 1, pp. 1–10, 2007.

[6] G. Arora and S. Sharma, "A comparative study of AA6351 mono-composites reinforced with synthetic and agro waste reinforcement," *International Journal of Precision Engineering and Manufacturing*, vol. 19, pp. 631–638, 2018.

[7] S. P. Dwivedi and A. K. Srivastava, "Utilization of chrome containing leather waste in development of aluminium based green composite material," *International Journal of Precision Engineering and Manufacturing-Green Technology*, vol. 7, pp. 781–790, 2020.

[8] H. Kumar, R. Prasad, P. Kumar, S. P. Tewari, and J. K. Singh, "Mechanical and tribological characterization of industrial wastes reinforced aluminum alloy composites fabricated via friction stir processing," *Journal of Alloys and Compounds*, vol. 831, Article ID 154832, 2020.

[9] S. P. Dwivedia, A. Saxena, S. Sharma, A. K. Srivastava, and N. K. Maurya, "Influence of SAC and eggshell addition in the physical, mechanical and thermal behaviour of Cr reinforced aluminium based composite," *International Journal of Cast Metals Research*, vol. 34, no. 1, pp. 43–55, 2021.

[10] S. Sarkar, A. Bhirangi, J. Mathew, R. Oyyaravelu, P. Kuppan, and A. S. S. Balan, "Fabrication characteristics and mechanical behavior of rice husk ash-silicon carbide reinforced Al-6061 alloy matrix hybrid composite," *Materials Today: Proceedings*, vol. 5, Part 2, no. 5, pp. 12706–12718, 2018.

[11] C. Hima Gireesh, K. G. Durga Prasad, K. Ramji, and P. V. Vinay, "Mechanical characterization of aluminium metal matrix composite reinforced with aloe vera powder," *Materials Today: Proceedings*, vol. 5, Part 1, no. 2, pp. 3289–3297, 2018.

[12] P. Samal, R. K. Mandava, and P. R. Vundavilli, "Dry sliding wear behavior of Al 6082 metal matrix composites reinforced with red mud particles," *SN Applied Sciences*, vol. 2, Article ID 313, 2020.

[13] B. Subramaniam, B. Natarajan, B. Kaliyaperumal, and S. J. S. Chelladurai, "Investigation on mechanical properties of aluminium 7075 - boron carbide - coconut shell fly ash reinforced hybrid metal matrix composites," *China Foundry*, vol. 15, pp. 449–456, 2018.

[14] A. Patil, N. R. Banapurmath, A. M. Hunashyal, and S. Hallad, "Enhancement of mechanical properties by the reinforcement of fly ash in aluminium metal matrix composites," *Materials Today: Proceedings*, vol. 24, Part 2, pp. 1654–1659, 2020.

[15] S. Jannet, R. Raja, S. Rajesh Ruban et al., "Effect of egg shell powder on the mechanical and microstructure properties of AA 2024 metal matrix composite," *Materials Today: Proceedings*, vol. 44, Part 1, pp. 135–140, 2021.

[16] R. Girimurugan, R. Pugazhenthi, T. Suresh, P. Maheskumar, and M. Vairavel, "Prediction of mechanical properties of hybrid aluminium composites," *Materials Today: Proceedings*, vol. 39, Part 1, pp. 712–716, 2021.

[17] N. Verma and S. C. Vettivel, "Characterization and experimental analysis of boron carbide and rice husk ash reinforced AA7075 aluminium alloy hybrid composite," *Journal of Alloys and Compounds*, vol. 741, pp. 981–998, 2018.

[18] S. P. Dwivedi, S. Sharma, and R. K. Mishra, "Microstructure and mechanical behavior of A356/SiC/fly-ash hybrid composites produced by electromagnetic stir casting," *Journal of the Brazilian Society of Mechanical Sciences and Engineering*, vol. 37, pp. 57–67, 2015.

[19] M. Challan, S. Jeet, D. K. Bagal, L. Mishra, A. K. Pattanaik, and A. Barua, "Fabrication and mechanical characterization of red mud based Al2025-T6 MMC using Lichtenberg optimization algorithm and Whale optimization algorithm," *Materials Today: Proceedings*, vol. 50, Part 5, pp. 1346–1353, 2022.

[20] F. O. Edoziuno, A. A. Adediran, B. U. Odoni, O. G. Utu, and A. Olayanju, "Physico-chemical and morphological evaluation of palm kernel shell particulate reinforced aluminium matrix composites," *Materials Today: Proceedings*, vol. 38, Part 2, pp. 652–657, 2021.

[21] M. Imran and A. R. Anwar Khan, "Characterization of Al-7075 metal matrix composites: a review," *Journal of Materials Research and Technology*, vol. 8, no. 3, pp. 3347–3356, 2019.

[22] P. Omoniyi, A. Adekunle, S. Ibitoye, O. Olorunpomi, and O. Abolusoro, "Mechanical and microstructural evaluation of aluminium matrix composite reinforced with wood particles," *Journal of King Saud University - Engineering Sciences*, vol. 34, no. 6, pp. 445–450, 2022.

[23] S. D. Saravanan and M. Senthil Kumar, "Effect of mechanical properties on rice husk ash reinforced aluminum alloy (AlSi10Mg) matrix composites," *Procedia Engineering*, vol. 64, pp. 1505–1513, 2013.

[24] A. Islam, S. P. Dwivedi, R. Yadav, and V. K. Dwivedi, "Development of aluminium based composite by utilizing industrial waste and agro-waste material as reinforcement particles," *Journal of the Institution of Engineers (India): Series D*, vol. 102, pp. 317–330, 2021.

[25] S. Arunkumar and A. Senthil Kumar, "Studies on egg shell and SiC reinforced hybrid metal matrix composite for tribological applications," *Silicon*, vol. 14, pp. 1959–1967, 2022.

[26] P. P. Ikubanni, M. Oki, A. A. Adeleke et al., "Tribological and physical properties of hybrid reinforced aluminium matrix composites," *Materials Today: Proceedings*, vol. 46, Part 12, pp. 5909–5913, 2021.

[27] J. Verma and H. Kumar, "Rice husk ash as reinforcement with aluminium metal matrix composite: a review of technique, parameter and outcome," in *Advances in Manufacturing and Industrial Engineering*, R. M. Singari, K. Mathiyazhagan, and H. Kumar, Eds., pp. 953–962, Springer, Singapore, 2021.

[28] A. K. Yadav, K. M. Pandey, and A. Dey, "Aluminium metal matrix composite with rice husk as reinforcement: a review," *Materials Today: Proceedings*, vol. 5, Part 3, no. 9, pp. 20130–20137, 2018.

[29] R. Yadav, V. K. Dwivedi, A. Islam, and S. P. Dwivedi, "Analysis of mechanical properties of Al-based metal matrix composite reinforced with ES and RHA," *World Journal of Engineering*, vol. 18, no. 6, pp. 930–937, 2021.

[30] M. Dhanashekar and V. S. Senthil Kumar, "Squeeze casting of aluminium metal matrix composites—an overview," *Procedia Engineering*, vol. 97, pp. 412–420, 2014.

[31] R. Arunachalam, S. Piya, P. K. Krishnan et al., "Optimization of stir–squeeze casting parameters for production of metal matrix composites using a hybrid analytical hierarchy process—Taguchi-Grey approach," *Engineering Optimization*, vol. 52, no. 7, pp. 1166–1183, 2020.

[32] S. Niyomwas, "Preparation of aluminum reinforced with TiB_2-Al_2O_3-Fe_xAl_y composites derived from natural ilmenite," *International Journal of Self-Propagating High-Temperature Synthesis*, vol. 19, pp. 150–156, 2010.

[33] J. V. Christy, R. Arunachalam, A.-H. I. Mourad, P. K. Krishnan, S. Piya, and M. Al-Maharbi, "Processing, properties, and microstructure of recycled aluminum alloy composites produced through an optimized stir and squeeze casting processes," *Journal of Manufacturing Processes*, vol. 59, pp. 287–301, 2020.

[34] T. Arunkumar, T. Selvakumaran, R. Subbiah, K. Ramachandran, and S. Manickam, "Development of high-performance aluminium 6061/SiC nanocomposites by ultrasonic aided rheo-squeeze casting method," *Ultrasonics Sonochemistry*, vol. 76, Article ID 105631, 2021.

[35] P. Chandrasekar and D. Nagaraju, "Improvement of bonding strength at the interfaces in scrap Al alloy composites using electroless Ni-P coated SiC," *Silicon*, vol. 14, pp. 2941–2952, 2022.

[36] M. Singh, R. S. Rana, R. Purohit, and K. Sahu, "Development and analysis of Al-matrix nano composites fabricated by ultrasonic assisted squeeze casting process," *Materials Today: Proceedings*, vol. 2, no. 4-5, pp. 3697–3703, 2015.

[37] M. Kok, "Production and mechanical properties of Al_2O_3 particle-reinforced 2024 aluminium alloy composites," *Journal of Materials Processing Technology*, vol. 161, no. 3, pp. 381–387, 2005.

[38] C. Kannan and R. Ramanujam, "Comparative study on the mechanical and microstructural characterisation of AA 7075 nano and hybrid nanocomposites produced by stir and squeeze casting," *Journal of Advanced Research*, vol. 8, no. 4, pp. 309–319, 2017.

[39] G. Liu, N. Zhao, C. Shi et al., "*In-situ* synthesis of graphene decorated with nickel nanoparticles for fabricating reinforced 6061Al matrix composites," *Materials Science and Engineering: A*, vol. 699, pp. 185–193, 2017.

[40] S. Kundu, S. K. Das, and P. Sahoo, "Tribological behaviour of electroless Ni-P deposits under elevated temperature," *Silicon*, vol. 10, pp. 329–342, 2018.

[41] P. Chandrasekar and D. Nagaraju, "Improvement of bonding strength at the interfaces in scrap Al alloy composites using electroless Ni-P coated SiC," *Silicon*, vol. 14, pp. 2941–2952, 2022.

[42] C. Fenghong, C. Chang, W. Zhenyu, T. Muthuramalingam, and G. Anbuchezhiyan, "Effects of silicon carbide and tungsten carbide in aluminium metal matrix composites," *Silicon*, vol. 11, pp. 2625–2632, 2019.

[43] R. Muraliraja and R. Elansezhian, "Effect of zwitterionic surfactant on tribological behaviour of electroless plating," *Surface Engineering*, vol. 30, no. 10, pp. 752–757, 2014.